PCCP

Chemical Design of Smart Chitosan/Polypyrrole/Magnetite Nanocomposite toward Efficient Water Treatment

Journal:	*Physical Chemistry Chemical Physics*
Manuscript ID:	CP-ART-07-2014-003062.R1
Article Type:	Paper
Date Submitted by the Author:	18-Aug-2014

Complete List of Authors:	Ayad, Mohamad M.; Department of Chemistry, Faculty of Science, University of Tanta, Tanta, Egypt, ; Salahuddin, Nehal; Faculty of Science, Tanta University, Department of Chemistry Fayed, Aya; Faculty of Science, Tanta University, Department of Chemistry Bishnu Prasad, Bastakoti; National Institute for Materials Science, WPI Center for MANA Suzuki, Norihiro Yamauchi, Yusuke; National Institute for Materials Science, WPI Center for MANA

Chemical Design of Smart Chitosan/Polypyrrole/Magnetite Nanocomposite toward Efficient Water Treatment

Mohamad Ayad,*[a] Nehal Salahuddin,[a] Aya Fayed,[a]
Bishnu Prasad Bastakoti,[b] Norihiro Suzuki,[c] and Yusuke Yamauchi*[b,d]

a *Department of Chemistry, Faculty of Science, University of Tanta, Tanta 31527 (Egypt)*

b *World Premier International (WPI) Research Center for Materials Nanoarchitectonics (MANA), National Institute for Materials Science (NIMS), 1-1 Namiki, Tsukuba, Ibaraki 305-0044 (Japan)*

c *International Center for Young Scientists (ICYS), National Institute for Materials Science (NIMS),1-2-1 Sengen, Tsukuba, Ibaraki 305-0047 (Japan)*

d *Faculty of Science and Engineering, Waseda University 3-4-1 Okubo, Shinjuku, Tokyo 169-8555 (Japan)*

*Corresponding authors: mayad12000@yahoo.com; Yamauchi.Yusuke@nims.go.jp

Abstract

Magnetic chitosan/polypyrrole/magnetite (Cs/PPy/Fe_3O_4) nanocomposite is prepared in a simple one-step method via *in-situ* chemical polymerization of pyrrole using anhydrous $FeCl_3$ as an oxidant in the presence of Cs. Magnetic Fe_3O_4 nanoparticles of size in the range of 10-20 nm are successfully introduced into the Cs/PPy matrix. Adsorption of an anionic dye (acid green 25, AG) from aqueous solution into the Cs/PPy/Fe_3O_4 nanocomposite is investigated. The nanocomposite exhibits high adsorption capacity compared to PPy and Cs themselves. After the adsorption, Cs/PPy/Fe_3O_4 nanocomposite is easily separated from the reaction solution using an external magnet, which is very useful for practical applications.

Keywords: Nanocomposite; Adsorbent; Polypyrrole; Chitosan; Acid green 25

1. Introduction

The interest in the synthesis of inorganic/organic nanocomposites has grown rapidly due to their wide range of applications in many fields. Conducting polymers, such as polyaniline (PANI) and polypyrrole (PPy), have been studied extensively[1-2]. PPy has triggered enormous research activities because of its fascinating features such as intrinsic high electrical conductivity and stability compared to the other conductive organic polymers.[3] In addition, PPy can be used in the fabrication of light emitting diode[4], polyFETs[5], EMI shielding[6], sensors[7], and anhydrous electro-rheological fluids[8]. It is more intriguing to explore the possibility of enhancing and/or extending the properties of conducting polymers by the formation of nanocomposites with inorganic materials such as magnetic iron oxides nanoparticles. The magnetic iron oxides (*e.g.*, maghemite (γ-Fe_2O_3) and magnetite (Fe_3O_4)) nanoparticles have recently gained increased interest due to their biocompatibility, strong super paramagnetic properties, and low toxicity[9]. Furthermore, the magnetic nanoparticles demonstrate promising applications in drug deli very, cell separation, biosensors, and enzymatic assays. Introducing these nanoparticles into the proper matrix can lead to high adsorption performance and removal of contaminants from aqueous solutions with easy magnetic separation and recovery from the medium by an external magnet[10].

Iron oxide nanoparticles have routinely been prepared by co-precipitation of aqueous solutions of Fe^{+2}/Fe^{+3} ions[9], solid state reaction[11], sol-gel method[12], hydrothermal process[13], ultrasonic method[14], and thermal decomposition.[15] However, iron oxide nanoparticles are prone to aggregate which limits their applications[16]. Many physical and chemical methods can be used to prevent or to minimize this drawback. One of these methods is to enwrap iron oxide nanoparticles into a polymer matrix. The polymer-iron oxide nanocomposites have been proved to possess unique electrical and ferromagnetic behavior and hence these nanocomposites have many potential applications[17-34]. For example, Diaz and Nguyen[18] have demonstrated that the *in-situ* polymerization of sodium pyrrole-*N*-propylsulfonate with $FeCl_3$ in water produces poly(pyrrole-*N*-propylsulfonate). Magnetic polymer nanocomposite containing

superparamagnetic γ-Fe_2O_3 particles were produced after treatment with aqueous NH_4OH. Additionally, Wan *et al.* have synthesized PANI and PPy composites containing iron oxide nanoparticles with excellent dispersion. The magnetic properties of the resulting composites showed ferromagnetic behavior (3.06-43.7 emu·g^{-1}) due to the presence of Fe_3O_4 nanoparticles with size range of 16-20 nm.[22-24] Chipara *et al.* have synthesized PPy/iron oxide nanocomposites by co-deposition of PPy and iron in the galvanostatic mode using square wave potentials[25]. Lim *et al.* have synthesized PPy/iron oxide nanocomposites by the *in-situ* oxidative polymerization of pyrrole in the presence of surface modified γ-Fe_2O_3 in supercritical carbon dioxide[26]. Similarly, PPy/Fe_3O_4 nanocomposites have also been synthesized by using the emulsion polymerization in aqueous solution[27].

In spite of the great interest and the large number of applications of PPy/iron oxide nanocomposites, the low adsorption characteristic is one of the major drawbacks of PPy-based nanocomposites, which hinders some of the practical applications[35]. Therefore, it is highly demanding to incorporate natural polymeric materials (*e.g.*, chitosan (Cs)) into PPy matrix, because such feature is highly desirable for efficient adsorption. Several reports have been devoted to the use of Cs-based adsorbents as a promising material for the removal of heavy transition metals and several dyes[36]. The combination of Cs and PPy is expected to improve the properties of both Cs and PPy especially the adsorption and the mechanical properties. There is still needed for an efficient dye adsorbent that possesses large capacity, fast separation, and easy recovery. Therefore, more attention has been paid for exploring and utilizing the immobilization of iron oxide nanoparticles into the Cs/PPy matrix. The addition of iron oxide is expected to result in the easy recovery during the removal of toxic ions and hazardous dyes from waste streams[37-40].

Herein, we present a facile synthetic route for the synthesis of Cs/PPy/Fe_3O_4 nanocomposite with supermagnetic behavior. Although similar Cs/PPy/Fe_3O_4 nanocomposite was reported by H. Bagheri *et al.*, they did not show the detailed characterization data. Here we show convincing characterization

data to confirm the successful formation of Cs/PPy/Fe_3O_4 nanocomposite. It was found that the Cs/PPy/Fe_3O_4 nanocomposite had a very high content of Fe_3O_4 nanoparticles, which were uniformly distributed without any aggregation[41]. A typical anionic dye (AG) was used as a model dye to investigate the adsorption properties of Cs/PPy/Fe_3O_4 nanocomposite and the adsorption behaviors and the isothermal kinetics were evaluated in detail. The synergic effects that combine the properties of PPy, Cs and uniformly dispersed Fe_3O_4, make the nanocomposite an ideal for AG dye removal with large capacity, fast adsorption rate, easy magnetic separation and recovery from the medium using a simple external magnet.

2. Experimental

2.1. Materials. Pyrrole (Mallinckrodt, USA) was purified by passing through a column of alumina neutral. Chitosan (Acros, USA, Molecular weight: 100,000-300,000), anhydrous $FeCl_3$ (SISCO, 98%), NaOH pellets (lobachemie), and acid green 25 (Aldrich) were used as received.

2.2. Synthesis of PPy. The PPy was prepared according to previous reports[42-44]. Briefly, 0.07 mole pyrrole was dissolved in 50 ml 0.1 M HCl. The solution was left stirred till homogenous solution was obtained. 50 ml of 0.174 M anhydrous $FeCl_3$ solution was added slowly to the acidic pyrrole solution, and then the reaction mixture was stirred for 1 h. The obtained PPy was then washed with distilled water several times and washed finally with methanol. The product was dried in an oven at 50 °C.

2.3. Synthesis of Cs/PPy/Fe_3O_4 nanocomposite. A solution of Cs (1 w/v) was prepared by dissolving 0.5 g Cs in 50 ml 2% (v/v) acetic acid. 0.25 ml of pyrrole was added to the Cs solution and the resulting solution was left stirred for 45 min. After that, 1.41 g anhydrous $FeCl_3$ was added to the Cs/pyrrole solution ($FeCl_3$/pyrrole ratio is 2.45) in an ice bath. The mixture was stirred overnight. NaOH solution was added slowly to the resulting solution. The obtained nanocomposite was washed by distilled water several times, then it was washed with methanol and collected by centrifugation. The Cs/PPy/Fe_3O_4 nanocomposite was finally left to dry in an oven at 50 °C for 2 days.

2.4. Characterizations. The morphology Cs/PPy/Fe_3O_4 nanocomposite was studied by scanning electron microscope (SEM) (Hitachi S4800) at an accelerating voltage of 5 kV and transmission electron microscope (TEM) (JEM-2100F) at 200 KV. X-ray diffraction (XRD) patterns were measured by GNR APD-2000 PRO diffractometer with Cu Kα radiation (40 KV, 30 mA) at a step scan mode. Fourier transform infrared spectra (FT-IR) were measured using Bruker, Tensor 27 FT-IR spectrophotometer with frequency range from 4000 cm^{-1} to 400 cm^{-1}. Thermogravimetric analysis (TGA) was carried out on Perkin Elmer, STA 6000. Saturation magnetization of Cs/PPy/Fe_3O_4

nanocomposite was measured by vibrating sample magnetometer (Lake Shore 7410). Raman spectra were measured by triple Raman spectrometer (Horiba) connected with spectra-physics beamlok laser unit. UV-visible absorption spectra were measured using UV spectrometer, UVD-2960 (Labomed Inc.).

3. Results and discussion

3.1. Synthesis of Cs/PPy/Fe_3O_4 nanocomposite.

The present study develops a simple and a convenient one-step process for the synthesis of Cs/PPy/Fe_3O_4 nanocomposite. The nanocomposite was prepared by the *in-situ* polymerization process of pyrrole using anhydrous $FeCl_3$ in the presence of Cs. Fe_3O_4 nanoparticles were formed in the Cs/PPy matrix, as illustrated in **Scheme 1**. Therefore, the resultant Cs/PPy/Fe_3O_4 nanocomposite possessed magnetic properties (The details are discussed later). Reduction of Fe^{III} to Fe^{II} was partially occurred during *in-situ* polymerization of pyrrole. The addition of NaOH converted the Fe cations (Fe^{III} and Fe^{II}) to the corresponding hydroxides ($Fe(OH)_3$ and $Fe(OH)_2$), finally forming the Fe_3O_4 nanoparticles (**Scheme 1**). Such method is crucial for the synthesis of novel Cs/PPy/Fe_3O_4 nanocomposite with uniformly distributed Fe_3O_4 nanoparticles even at a very high content of Fe_3O_4.

Fig. 1 shows the XRD patterns of Cs/PPy/Fe_3O_4 nanocomposite as well as those of the parent PPy and Cs. A broad peak at 22.8º indicates that the PPy is in the amorphous form (**Fig. 1a**)[26]. The XRD pattern of Cs (**Fig. 1b**) shows two characteristic peaks at 9.9º and 20.3º. The presence of plenty of -OH and -NH_2 groups in Cs structure forms strong inter- and intra-molecular hydrogen bonds, thereby showing certain regularity in Cs structure[45,46]. In the case of Cs/PPy/Fe_3O_4 nanocomposite (**Fig. 1c**), several diffraction peaks were observed. These peaks were assigned to be (111), (220), (311), (400), (422), (511), (440), (620), and (622) of crystalline Fe_3O_4 phase[47,48]. Compared to bulk Fe_3O_4 crystal, the very broad peaks indicate the small crystallite size. The average crystalline size of Fe_3O_4 nanoparticles was roughly calculated according to Scherrer equation[49]. The highest three peaks were selected for this calculation. The average crystalline size was found to be about 10 nm.

The morphology of Cs/PPy/Fe_3O_4 nanocomposite was characterized by SEM and TEM observations. The SEM image in **Fig. 2a** shows that the nanocomposites are in spherical shape and

their sizes are in the range from 50 nm to 100 nm. It has been reported that the polymerization of pyrrole with anhydrous $FeCl_3$ in acidic medium produces course particles with spherical shape[37]. TEM image in **Fig. 2b** shows that the Fe_3O_4 nanoparticles are well dispersed without any serious aggregation. A high-resolution TEM image confirms the existence of crystallized Fe_3O_4 nanoparticles (**Fig. 2b**). The sizes of the nanoparticles are varied from 5 to 20 nm, which is almost consistent with the size estimated from XRD data. Lattice fringes are coherently extended on each nanoparticle, indicating that each particle has a single crystalline structure (inset of **Fig. 2b**). Selected-area electron diffraction (SAED) patterns taken from 10,000 nm^2 (100 nm × 100 nm) showed ring-like pattern which can be indexed as (111), (220), (311), (400), and (422) diffractions of Fe_3O_4 crystals (not shown). Although each nanoparticle shows single crystalline structure, all the nanoparticles are randomly oriented inside the polymer matrix. Therefore, the ED patterns taken from 10,000 nm^2 showed a polycrystalline nature.

The uniformly dispersed Fe_3O_4 nanoparticles in the Cs/PPy matrix were further visualized by TEM elemental mapping (**Fig. 3**). High-angle annular dark-field scanning transmission electron microscope (HAADF-STEM) image confirms the presence of Fe_3O_4 nanoparticles. The elemental mapping of carbon, oxygen, and iron are shown in **Fig. 3b-d**. From energy dispersive X-ray spectroscopic (EDX) analysis, it was found that the total nanocomposite is composed of carbon, nitrogen, oxygen, and iron (**Fig. S1**). From the above SEM and TEM observations; it was proved that Cs/PPy/Fe_3O_4 nanocomposite was successfully synthesized without any aggregation of nanoparticles.

To investigate the weight loss of Cs/PPy/Fe_3O_4 nanocomposite, TGA measurement was performed under nitrogen atmosphere. Three steps weight loss was observed (**Fig. 4**). The first step from 40 ºC to 165 ºC can be attributed to the loss of moisture from the polymer structure. The second weight loss observed from 165 ºC to 317 ºC is typical to the degradation of Cs, while the third weight loss between 317 ºC to 488 ºC can be assigned to the decomposition of the PPy main chain. The total

weight loss is 53.5%, thus the residue of Fe_3O_4 is 44.5% and this percentage is close to the Fe content obtained from the elemental mapping data.

The composition of Cs/PPy/Fe_3O_4 nanocomposite was further characterized by FT-IR spectroscopy (**Fig. 5c**). FTIR spectra of PPy (**Fig. 5a**) and Cs (**Fig. 5b**) were also shown for comparison. N-H stretching vibration at 3448 cm^{-1} of PPy and O-H axial stretching vibration band at 3433 cm^{-1} of Cs are shifted in the FT-IR spectrum of Cs/PPy/Fe_3O_4 nanocomposites to become a broad peak at 3355 cm^{-1} (**Fig. 5c**). The Cs peak, which is observed at 1643 cm^{-1} in **Fig. 5b**, totally disappears and the PPy peak, which is observed at 1546 cm^{-1} in **Fig. 5a** is shifted to 1558 cm^{-1}. Thus, the spectrum of the nanocomposite (**Fig. 5c**) comprises the main peaks of both PPy and Cs with some shifting due to the effective interaction between PPy and Cs. Similar results have also been reported by Khor *et al*.[50]. The peaks at 1558 cm^{-1} and 1464 cm^{-1} suggest that the Cs/PPy is coated onto Fe_3O_4 nanoparticles[51]. The presence of Fe_3O_4 nanoparticles in the nanocomposite is strongly supported by the new peak at 570 cm^{-1} which is a characteristic to Fe_3O_4[51,52]. The shifting of characteristic peak of pure Fe_3O_4 nanoparticles due to the Fe-O bond (584 cm^{-1}-580 cm^{-1})[53,54] to 570 cm^{-1} indicates the electrostatic interaction between the negatively charged Fe_3O_4 surface and the positively protonated amino groups in the Cs and PPy. From the above results, it is proved that the Fe_3O_4 nanoparticles and the Cs/PPy are successfully integrated into Cs/PPy/Fe_3O_4 nanocomposite. The interaction between Fe_3O_4 nanoparticles and Cs/PPy can be further confirmed by Raman spectroscopy (**Fig. 6**). There is a shift of the characteristic bands of pure Fe_3O_4 nanoparticles at 668 cm^{-1} and 532 cm^{-1} to 627 cm^{-1} and 450 cm^{-1}, respectively, indicating that the electrostatic interaction between Fe_3O_4 surface and the protonated amino group of Cs/PPy[55].

To explore the potential applications of Cs/PPy/Fe_3O_4 nanocomposite, the magnetic properties were also studied in detail. A typical magnetization curve as a function of the applied field at room

temperature is shown in **Fig. 7**. The nanocomposite has a magnetic saturation moment (M_s) of 28.96 emu·g^{-1}. The absence of hysteresis loop (H_c=0) indicates the superparamagnetic nature with no permanent magnetic moment. The high M_s value observed here apparently originated from the large loading amount of magnetic Fe_3O_4 nanoparticles. Such superparamagnetic nanocrystals are believed to be promising adsorbent for waste water treatment, as their dispersion in solvents can be easily separated by applying an external magnetic field.

3.2. Adsorption of AG onto Cs/PPy/Fe_3O_4 nanocomposite

The magnetic Cs/PPy/Fe_3O_4 nanocomposite can be utilized as an ideal material for waste water treatment. A typical anionic dye, AG was used as a model dye. A stock solution of AG dye was prepared in distilled water and the necessary dilution was made to get the required concentration of working solution. AG solutions (50 ml) of same concentrations were mixed with 0.05 g PPy, Cs or Cs/PPy/Fe_3O_4 nanocomposite and stirred at 400 rpm in the dark at room temperature. The supernatant solution was taken at predetermined time intervals. The remaining dye concentration in the supernatant solution was evaluated spectrophotometrically at 642 nm.

The amount of AG adsorbed onto the Cs/PPy/Fe_3O_4 nanocomposite samples was calculated by subtracting the final solution concentration from the initial concentration of dye solutions. The amount of dye adsorbed onto a unit weight of the nanocomposite, Q_e (mg·g^{-1}) was calculated by using mass balance equation[56].

$$Q_e = \frac{(C_0 - C_e)V}{m} \quad (1)$$

where C_o is the initial dye concentration in liquid phase (mg·L^{-1}), C_e is the liquid phase dye concentration at equilibrium (mg·L^{-1}), V is the volume of dye solution used (L), and m is the mass of adsorbent used (mg). The dye removal efficiency percentage (*RE%*) of AG adsorbed onto the Cs/PPy/Fe_3O_4 nanocomposite was calculated from the given equation[56].

$$RE\% = \frac{(C_0 - C_e)}{C_0} \times 100 \quad (2)$$

where C_o is the initial dye concentration (mg·L^{-1}), and C_e is the dye concentration at equilibrium (mg·L^{-1}).

It is clearly found that the Cs/PPy/Fe_3O_4 nanocomposite possess impressive high adsorption rate with adsorption capacities of 26.2 mg·g^{-1} for AG, which are higher than that of the pristine Cs

(22.8 mg·g^{-1}) and the PPy (19.79 mg·g^{-1}) as shown in **Fig. 8**. Considering that the content of Cs/PPy is only 55% of Cs/PPy/Fe_3O_4 nanocomposite, the adsorption capacity of Cs/PPy/Fe_3O_4 nanocomposite is overwhelmingly high. The dye removal efficiency using Cs/PPy/Fe_3O_4 nanocomposite reaches 96.6% in 60 min which can be attributed to the large number of binding sites due to strong interaction between AG and the Cs/PPy/Fe_3O_4 nanocomposite. In acidic condition (pH = 5.4), the protonation of -NH_2 and -NH- groups of Cs/PPy/Fe_3O_4 nanocomposite to -NH_3^+ and -NH_2^+- promote the electrostatic interaction with O^- in AG, in addition to the hydrogen bonding between -OH in the Cs skeleton and -NH group of AG. The synergic effects that combine the properties of PPy, Cs and uniformly dispersed Fe_3O_4, make the nanocomposite ideal for AG dye removal with large capacity with fast adsorption rate, easy magnetic separation, and recovery from the medium using a simple external magnet. After the dye adsorption, the nanocomposites can be easily collected by external magnet (**Fig. 9**).

In order to study the adsorption kinetics, pseudo-first order[57], pseudo-second order[58], and intraparticle diffusion[59] models were evaluated. For kinetic study, 27.8 mg·L^{-1} dye solution (50 ml) was mixed with 0.05 g of PPy, Cs, or Cs/PPy/Fe_3O_4 nanocomposite in the dark at 25 °C.

Pseudo-first order rate equation: $\log(Q_e - Q_t) = \log Q_e - \frac{k_1}{2.303} t$ (4)

Pseudo-second order equation: $t/Q_t = 1/k_2 Q_e^2 + t/Q_e$ (5)

Intraparticle diffusion model: $Q_t = k_3 t^{1/2} + C$ (6)

where Q_e and Q_t refer to the amount of dye adsorbed at equilibrium and time t, respectively, k_1, k_2 and k_3 are the rate constant for pseudo-first order, pseudo-second order and intraparticle diffusion model. C is a constant. The validity of the models was verified by the linear equation analysis of $\log(Q_e\text{-}Q_t)$ *vs.* t, (t/Q_t) *vs.* t and Q_t *vs.* $t^{1/2}$, respectively (**Fig. S2**). The kinetic parameter of pseudo-first order, pseudo second order, and intraparticle diffusion model are summarized in **Table 1.** Good correlation with the kinetic data explains the dye adsorption mechanism in solid phase. The fitting with excellent linearity

and the highest correlation coefficient ($R^2 = 0.997$) confirms the applicability of the pseudo-first order equation. The theoretical value of Q_e (26.2 mg·g^{-1}) is very close to the experimental Q_e (27.6 mg·g^{-1}) value. This is also correlated with Chi-square (χ^2) test. The Chi-square test statistic is basically the sum of the squares of the differences between the experimental data and the data obtained by calculation from models, with each squared difference divided by the corresponding data obtained by calculation from models.[36] The equivalent mathematical statement is

$$\chi^2 = \sum_{i=1}^{m} \frac{\left(q_{e,\exp} - q_{e,calc}\right)^2}{q_{e,\exp}} \quad (7)$$

where, $q_{e,exp}$ and $q_{e,cal}$ are equilibrium capacity (mg·g^{-1}) for experimental and calculated using different models. If the data from the model are similar to experimental data, χ^2 will be small. If they differ, χ^2 will be large. χ^2 value for each model is shown in **Table 1** which is correlated with correlation coefficient result and obeys pseudo-first order.

Adsorption isotherms provide information for analyzing and designing an adsorption process. Hence, the correlation of equilibrium data using either a theoretical or empirical equation is essential for the interpretation and the prediction of the extent of adsorption. The adsorption isotherms of the adsorption of AG into Cs/PPy/Fe_3O_4 nanocomposite were also studied. The most common sorption models used to fit the experimental data are Langmuir[60], Freundlich[61], and Temkin[62] isotherm equations as follows.

Langmuir: $C_e/Q_e = 1/K_\ell + a_\ell C_e/K_\ell$ (8)

Freundlich: $\ln Q_e = \ln K_f + (1/n)\ln C_e$ (9)

Temkin: $Q_e = B \ln K_t + B \ln C_e$ (10)

where, C_e is the equilibrium concentration of the adsorbate, K_1 and a_1 are Langmuir constants, K_f and n are Freundlich constants, K_t and B are Temkin constants. The equilibrium data obtained were fitted to

the above three isotherm equations separately and the parameters were evaluated (**Table 2**) along with the correlation coefficients' values for each fit (**Fig. S3**). The linear correlations' coefficients shows that the Freundlich isotherm preferably fits the AG adsorption data on Cs/PPy/Fe_3O_4 nanocomposite.

4. Conclusion

We successfully developed a facile and one-step route to synthesize a magnetic Cs/PPy/Fe_3O_4 nanocomposite by *in-situ* polymerization of pyrrole using $FeCl_3$ as an oxidant in the presence of Cs. This process is imperative in order to avoid the unwanted nanoparticle aggregation. Highly crystalline and uniformly-distributed Fe_3O_4 nanocrystals with size range of 5-20 nm were incorporated into the Cs/PPy matrix. The synthesized Cs/PPy/Fe_3O_4 nanocomposite showed a strong magnetic response. The synergic effect that combines the properties of PPy, Cs and uniformly distributed Fe_3O_4 nanoparticles make the nanocomposite an ideal adsorbent for AG dye. The adsorption kinetics follows the pseudo-first order model and the equilibrium data preferably fits to the Freundlich model. The large adsorption capacity, fast adsorption rate, and easy magnetic separation make the Cs/PPy/Fe_3O_4 nanocomposite a highly promising adsorbent for environmental sanitation. Recently, mesoporous materials prepared through surfactant assembly[63-67] have attracted great interest as another promising adsorbent for dyes[68-73]. Compare to these mesoporous materials, inorganic/organic nanocomposites can be easily synthesized without any complicated synthetic processes. Here we demonstrate easy synthetic protocol for novel inorganic/organic nanocomposites which can be extended to other functional nanocomposites useful for environmental remediation in future.

References

[1] J. Anand, S. Palaniappan and D. Sathyanarayana, *Prog. Polym. Sci*. 1998, **23**, 993.

[2] M. Karthikeyan, K. K. Satheesh Kumar, K. P. Elango, *Desalination* 2011, **267**, 49.

[3] R. Potember, R. Hoffman, H. Hu, J. Cocchiaro, A. Viands, R. Murphy and T. Poehler, *J. Polym*. 1987, **28**, 574.

[4] P. Kilmartin and G. Wright, *Electrochim. Acta*. 2001, **46**, 2787.

[5] J. Hatfield, J. Covington and J. Gardner, *Sens. Actuators, B.* 2000, **65**, 253.

[6] C. Lee, D. Lee, J. Joo, M. Kim, J. Lee, S. Jeong and S. Byun, *Synth. Met*. 2001, **119**, 429.

[7] Y. Liu, B. Hwang and Y. Chen, *Electroanalysis*. 2002, **14**, 556.

[8] J. Goodwin, G. Markham and B. Vincent, *J. Phys. Chem*. 1997, **101**, 1961.

[9] T. Pisanic, J. Blackwell, V. Shubayev, R. Finones and S. Jin, *Biomater.* 2007, **28**, 2572.

[10] S. Armes, *Synth. Met*. 1987, **20**, 365.

[11] G. Chandrasekaran and P. Sebastian, *Mater. Lett*. 1998, **37**, 17.

[12] W. Kim, S. Kim, S. Lee and C. Kim, *J. Magn. Magn. Mater.* 2001, **226**, 1418.

[13] B. P. Bastakoti, K. C.-W. Wu, H. Sukegawa and Y. Yamauchi, *RSC Adv.,* 2014, **4**, 9986.

[14] X. Lu, H. Mao, D. Chao, W. Zhang and Y. Wei, *J. Solid State Chem*. 2006, **179**, 2609.

[15] Y. Chen, D. L. Peng, D. Lin and X. Luo, *Nanotechnology*, 2007, **18**, 505703.

[16] R. Hong, B. Feng, G. Liu, S. Wang, H. Li, V. Ding, V. Zheng and D. Wei, *J. Alloys Compd*. 2009, **476**, 612.

[17] G. Li, Y. Jiang, K. Huangb, P. Ding and J. Chen, *J. Alloys Compd*. 2008, **466**, 451.

[18] T. Nguyen and A. Diaz, *Adv. Mater*. 1994, **6**, 858.

[19] R. Shull and L. Bennett, *Nanostruct. Mater*. 1992, **1**, 83.

[20] J. Sinfelt, *Science.* 1977, **195**, 641.

[21] T. Xiao, Y. Zhang, P. Strutt, J. Budrick, K. Mohan and K. Gonsalves, *Nanostruct. Mater*. 1993, **2**, 285.

[22] J. Liu and M. Wan, *J. Polym. Sci., Part A: Polym. Chem*. 2000, **38**, 2734.

[23] M. Wan and J. Fan, *J. Polym. Sci., Part A: Polym. Chem*. 1998, **36**, 2749.

[24] M. Wan, J. Li and S. Li, *J. Appl. Polym. Sci*. 1996, **61**, 793.

[25] M. Chipara, R. Skomski and D. Sellmyer, *Mater. Lett*. 2007, **61**, 2412.

[26] H. Yuvaraj, M. Woo, E. Park, Y. Jeong and K. Lim, *Eur. Polym. J.* 2008, **44**, 637.

[27] R. Tandon, M. Tripathy, A. Arora and S. Hotchandan, *Sens. Actuators, B*. 2006, **114**, 768.

[28] J. Cao, J. Li, L. Liu, A. Xie, S. Li, L. Qiu, Y. Yuan and Y. Shen, *J. Mater. Chem. A* 2014, **2**, 7953.

[29] Y. Wang, B. Zou, T. Gao, X. Wu, S. Lou and S. Zhou, *J. Mater. Chem.* 2012, **22**, 9034.

[30] X. Han, L. Gai, H. Jiang, L. Zhao, H. Liu and W. Zhang, *Synth. Met.* 2013, **171**, 1.

[31] D. H. K. Reddy and S. M. Lee, *Adv. Colloid Interface Sci.* 2013, **201-202**, 68.

[32] R. Xiong, Y. Wang, X. Zhang and C. Lu, *RSC Adv.* 2014, **4**, 22632.

[33] P. Wang, T. Yan and L. Wang, *BioResources* 2013, **8**, 6026.

[34] Y. Zhou, S. Fu, L. Zhang, H. Zhan and M. V. Levit, *Carbohyd. Polym.* 2014, **101**, 75.

[35] R. Ansari and Z. Mosayebzadeh, *J. Iran. Chem. Soc*. 2010, **7**, 339.

[36] G. Annadurai, L. Ling and J. Lee, *J. Hazard. Mater*. 2008, **152**, 337.

[37] M. Bhaumika, T. Leswifi, A. Maity, V. Srinivasu and M. Onyango, *J. Hazard. Mater*. 2011, **186**, 150.

[38] A. Kaushik, P. Solanki, A. Ansari, S. Ahmad and B. Malhotra, *Electrochem. Commun*. 2008, **10**, 1364.

[39] A. Nan, R. Turcu, I. Bratu, C. Leostean, O. Chauvet, E. Gautron and J. Liebscher, *Akrivoc*. 2010, **X**, 185.

[40] H. Zhu, R. Jiang, L. Xiao and W. Li, *J. Hazard. Mater*. 2010, **179**, 251.

[41] H. Bagheri, A. Roostaie, M. Y. Baktash, *Anal. Chem. Acta* 2014, **816**, 1.

[42] M. Ayad, *J. Mater Sci.* 2009, **44**, 6392.

[43] M. Ayad, *J. Appl. Polym. Sci*. 1994, **53**, 1331.

[44] S. Machida, S. Miyata and A. Techagumpuch, *Synth. Met.* 1989, **31**, 311.

[45] S. Govindan, E. Nivethaa, R. Saravanan, V. Narayanan and A. Stephen, *Appl. Nanosci*. 2012, **2**, 299.

[46] R. Ramya, P. Sudha and J. Mahalakshmi, *Inter. J. Sci. Res. Publ*. 2012, **2**, 1.

[47] M. Bhaumika, T. Leswifi, A. Maity, V. Srinivasu and M. Onyango, *J. Hazard. Mater*. 2011, **190**, 381.

[48] K. Suri, S. Annapoorni and R. Tandon, *Mater. Sci*. 2001, **24**, 563.

[49] C. Hammond, *The Basics of Crystallography and Diffraction*, Oxford University Press: Oxford, United Kingdom, 3rd edition 1997.

[50] E. Khor and J. Hee, *Carbohydr. Polym*. 1995, **26**, 183.

[51] X. Luo, X. Song, A. Zhu, Y. Si, L. Ji, V. Ma, Z. Jiao and J. Wu, *J. Mater. Sci. Mater. Med*. 2012, **23**, 3075.

[52] Y. Li, J. Church and A. Woodhead, *J. Magn. Magn. Mater*. 2012, **324**, 1543.

[53] K. Elwakeel, A. Atia and A. Donia, *Hydrometallurgy*. 2009, **97**, 21.

[54] J. Sun, S. Zhou, P. Hou, Y. Yang, J. Weng, X. Li, M. Li, *J. Biomed. Mater. Res. Part A*. 2007, **80**, 332.

[55] R. M. Cornell and U. Schwertmann, *The Iron Oxide: Structure, Properties, Reactions, Occurrence and Uses*. WILEY-VCH, Weinheim, 2nd, 2004.

[56] N. Amin, *J. Hazard. Mater*. 2009, **165**, 52.

[57] Y. Ho, *J. Hazard. Mater. B.* 2006, **136**, 681.

[58] Y. Ho, and G. McKay, *Process Biochem*, 1999, **34**, 451.

[59] I. Uzun, *Dyes Pigm*. 2006, **70**, 76.

[60] I. Langmuir, *J. Am. Chem. Soc*. 1918, **40**, 1361.

[61] H. Z. Freudlich, *J. Phys. Chem.* C. 1906, **57**, 385.

[62] M. Temkin and V. Pyzhev, *Acta Physiochim.* 1940, **12**, 217.

[63] K. Ariga, A. Vinu, Y. Yamauchi, Q. Ji, J. P. Hill, *Bull. Chem. Soc. Jpn.* 2012, **85**, 1.

[64] Y. C. Lee, C. T. Chen, Y. T. Chiu and K. C. W. Wu, *ChemCatChem* 2013, **5**, 2153.

[65] K. Ariga, Y. Yamauchi, G. Rydzek, Q. Ji, Y. Yonamine, K. C. W. Wu, J. P. Hill, *Chem. Lett.* 2014, **43**, 36.

[66] W. H. Peng, Y. Y. Lee, C. Wu and Kevin C. W. Wu, *J. Mater. Chem.* 2012, **22**, 23181.

[67] Y. Yamauchi, *J. Ceram. Soc. Jpn.* 2013, **121**, 831.

[68] Y. Yamauchi, N. Suzuki, K. Sato, N. Fukata, M. Murakami and T. Shimizu, *Bull. Chem. Soc. Jpn.* 2009, **82**, 1039.

[69] T. Yokoi, T. Tatsumi and H. Yoshitake, *Bull. Chem. Soc. Jpn.* 2003, **76,** 2225.

[70] H. Yoshitake, T. Yokoi and T. Tatsumi, *Bull. Chem. Soc. Jpn.* 2003, **76**, 847.

[71] N. Suzuki, P. Gupta, H. Sukegawa, K. Inomata, S. Inoue and Y. Yamauchi, *J. Nanosci. Nanotechnol.* 2010, **10**, 6612.

[72] N. Suzuki and Y. Yamauchi, *J. Nanosci. Nanotechnol.* 2010, **10**, 5759.

[73] M. Paul, N. Pal and A. Bhaumik, *Mater. Sci. Eng. C* 2012, **32**, 1461.

Scheme 1

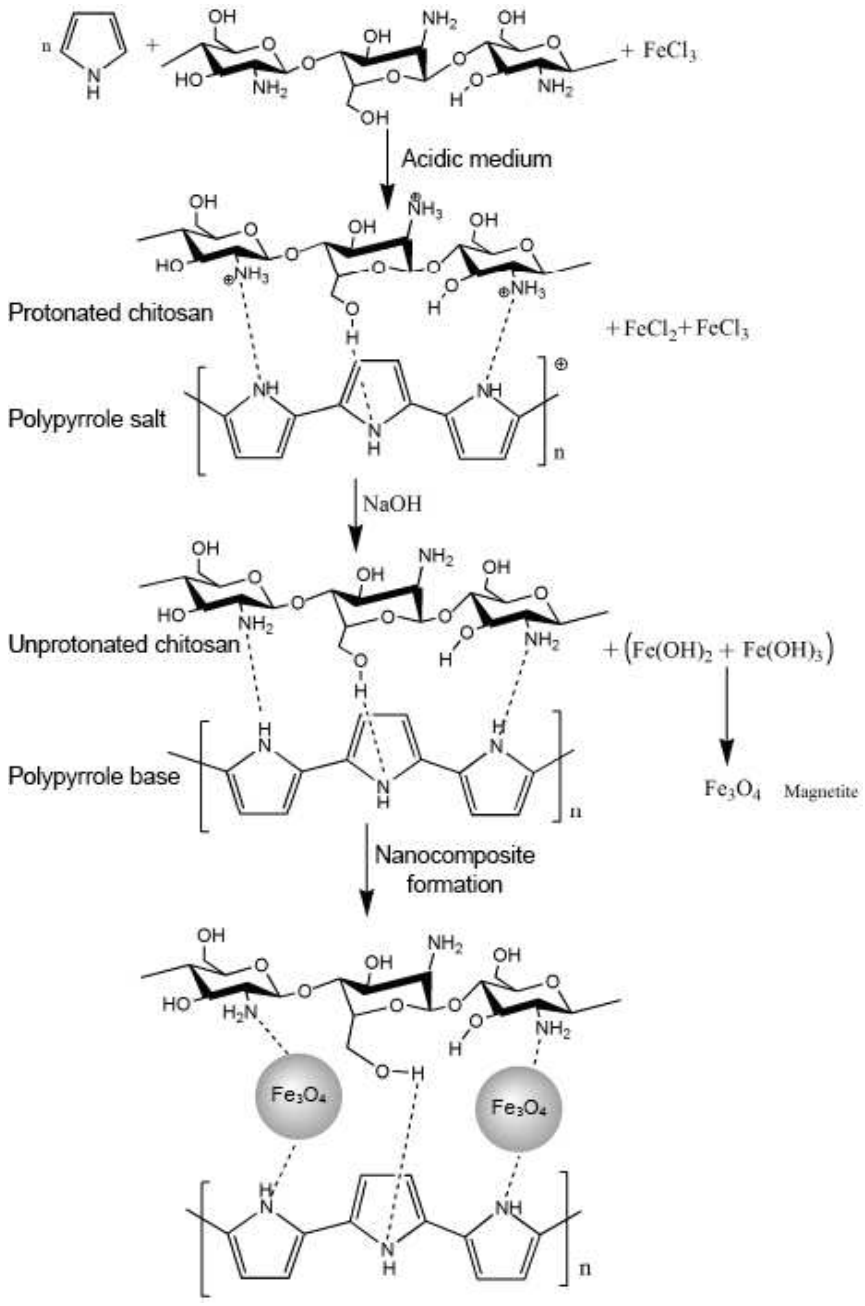

Scheme 1. The mechanism shows the *in-situ* polymerization of PPy into Cs solution followed by the *in-situ* formation of Fe_3O_4 in Cs/PPy matrix.

Fig. 1

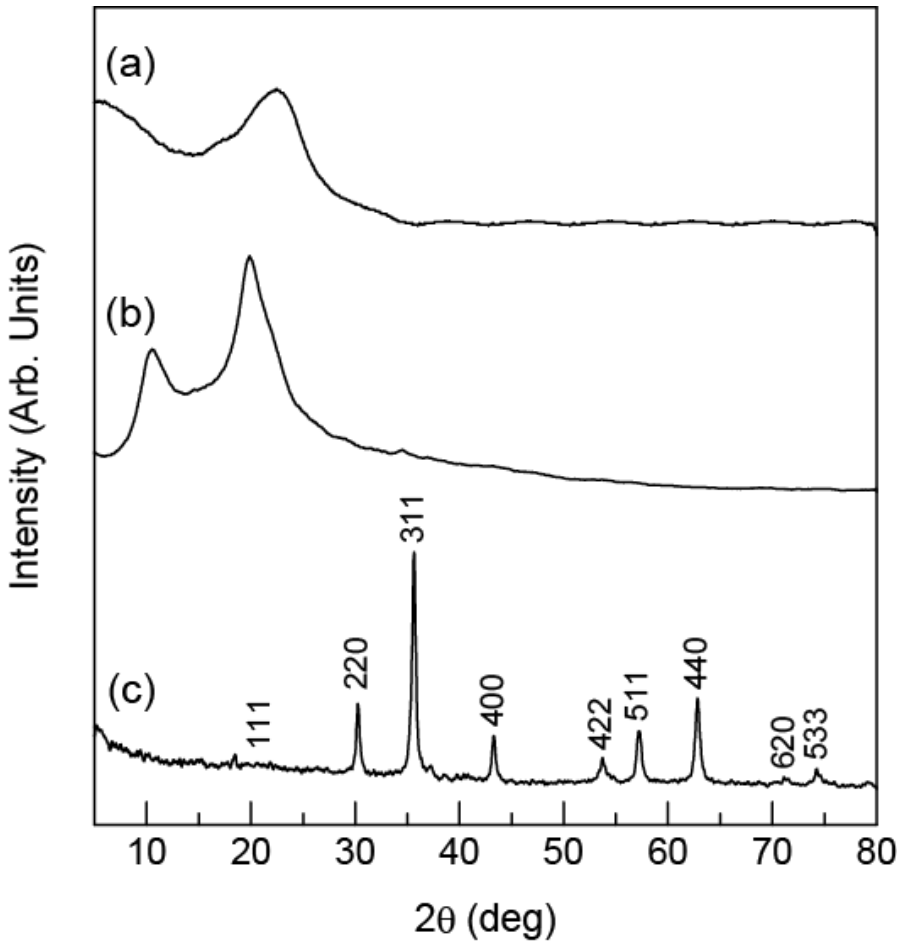

Fig. 1 XRD patterns of (a) PPy, (b) Cs, and (c) Cs/PPy/Fe_3O_4 nanocomposite.

Fig. 2

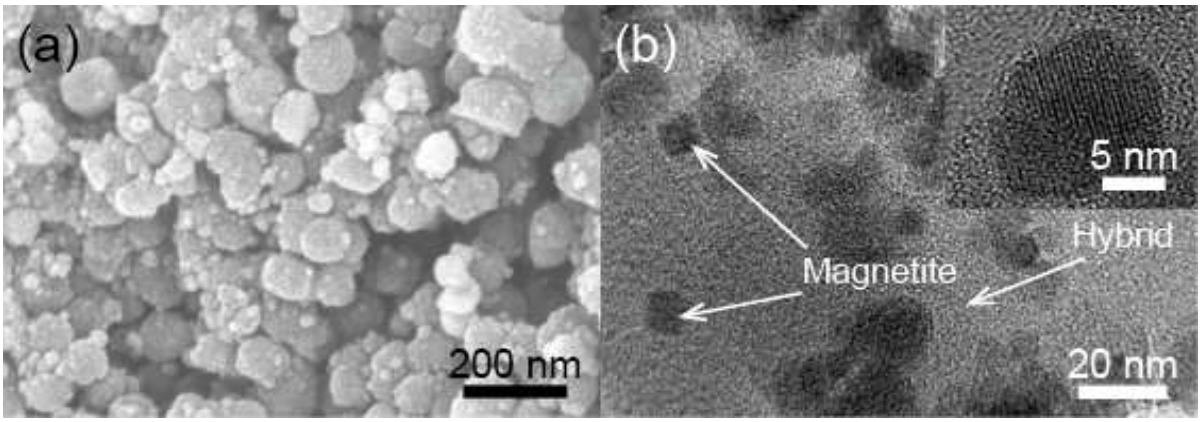

Fig. 2 (a) SEM and (b) TEM images of the Cs/PPy/Fe_3O_4 nanocomposite. Inset shows high resolution TEM image of the deposited Fe_3O_4 nanoparticle.

Fig. 3

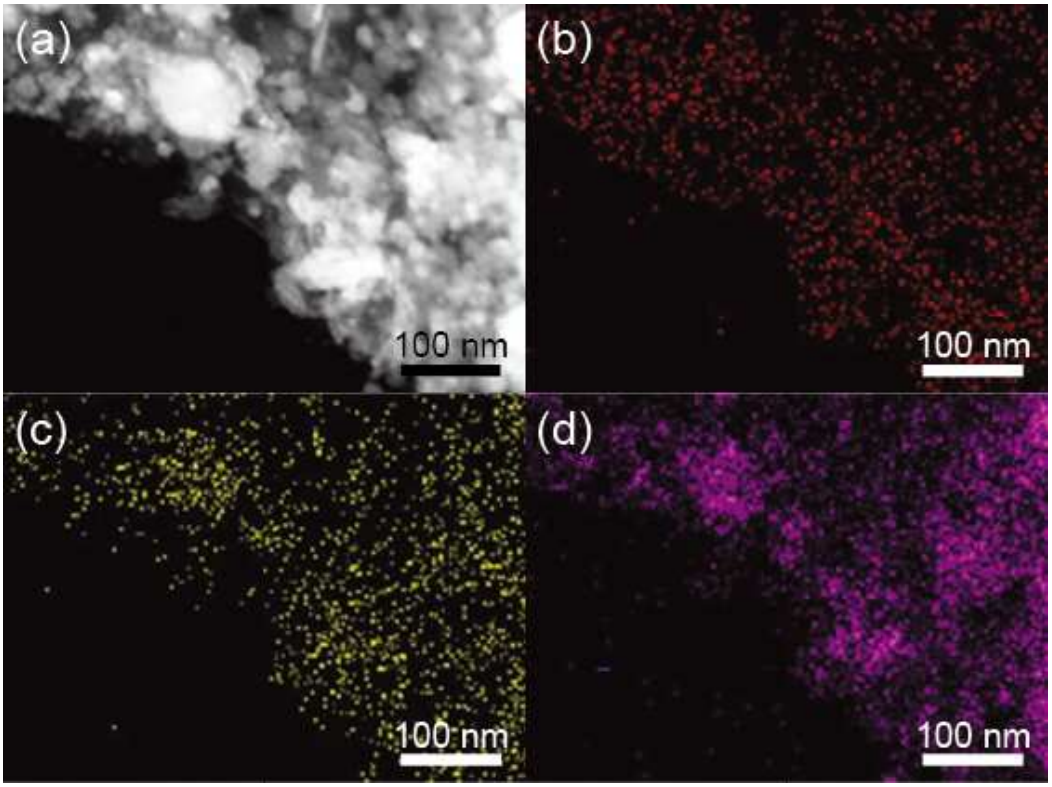

Fig. 3 (a) HAADF-STEM image of Cs/PPy/Fe_3O_4 nanocomposite and (b-d) elemental mapping of (b) C, (c) O, and (d) Fe.

Fig. 4

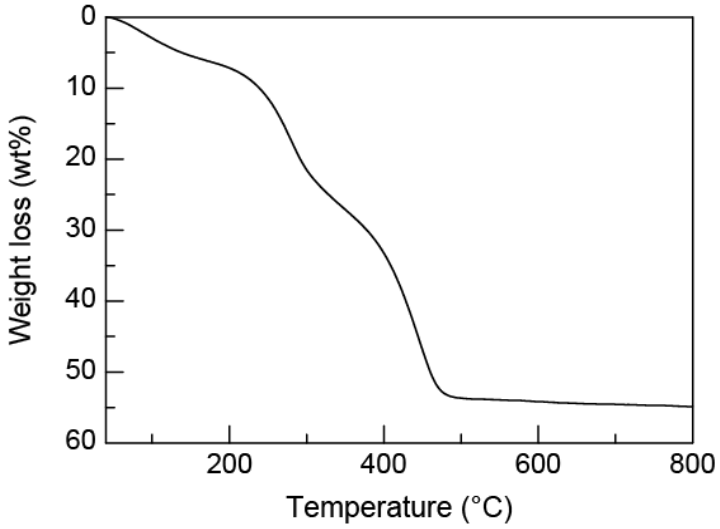

Fig. 4 Thermogravimetric analysis of Cs/PPy/Fe_3O_4 nanocomposite.

Fig. 5

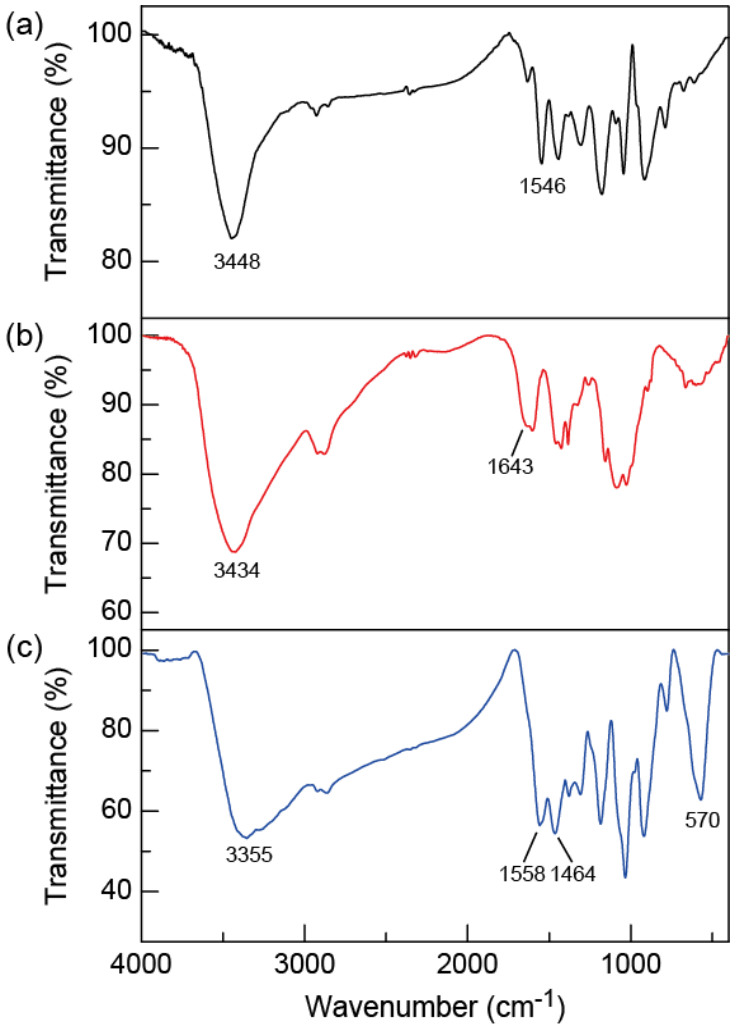

Fig. 5 FT-IR spectra of (a) PPy, (b) Cs, and (c) Cs/PPy/Fe_3O_4 nanocomposite.

Fig. 6

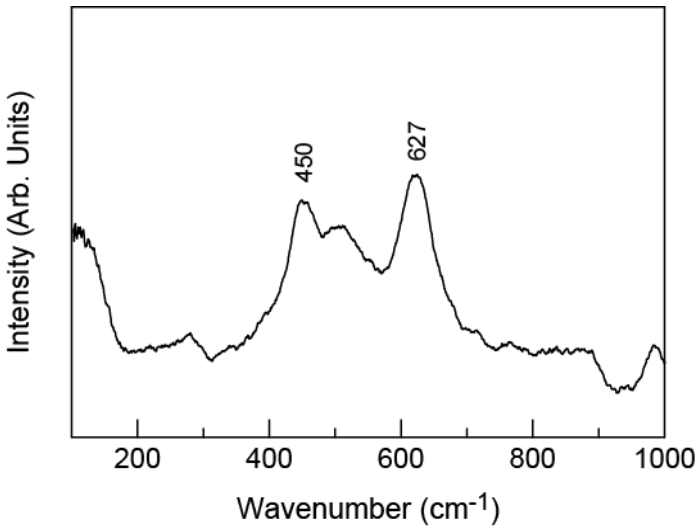

Fig. 6 Raman spectrum of Cs/PPy/Fe_3O_4 nanocomposite.

Fig. 7

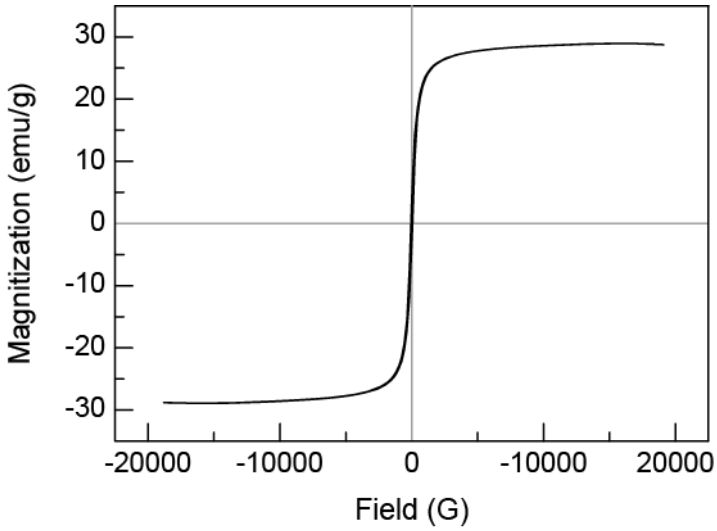

Fig. 7 Magnetization curves for Cs/PPy/Fe_3O_4 nanocomposite at room temperature.

Fig. 8

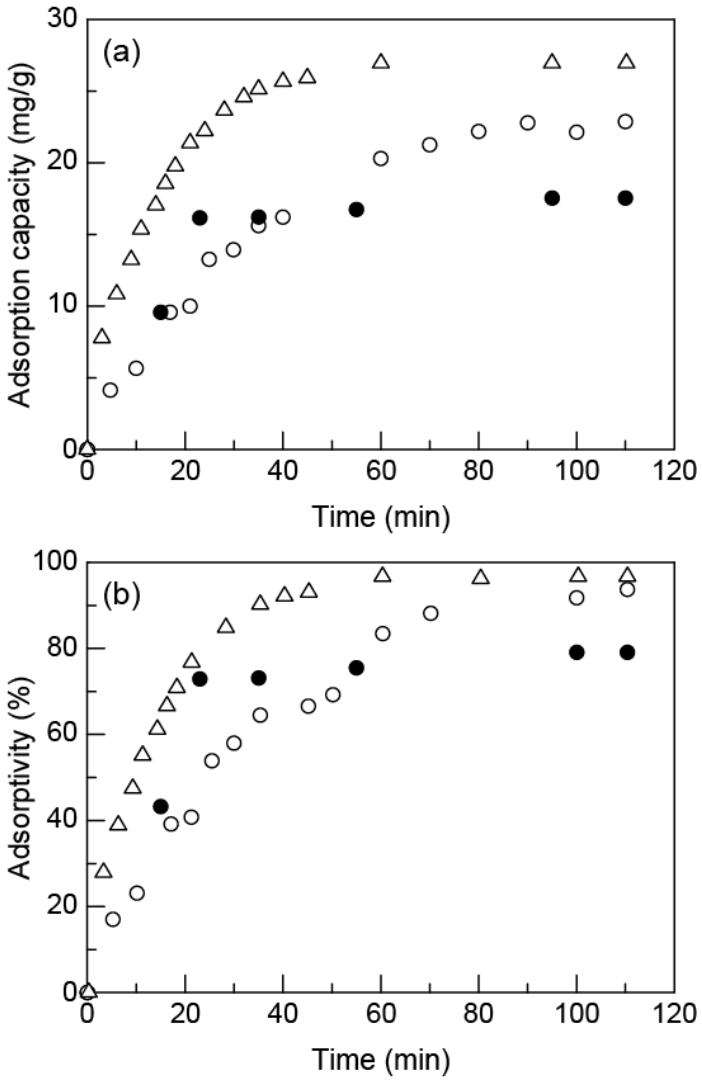

Fig. 8 (a) Adsorption capacity and (b) adsorptivity of (o) Cs, (●) PPy, and (Δ) Cs/PPy/Fe_3O_4 nanocomposite for AG.

Fig. 9

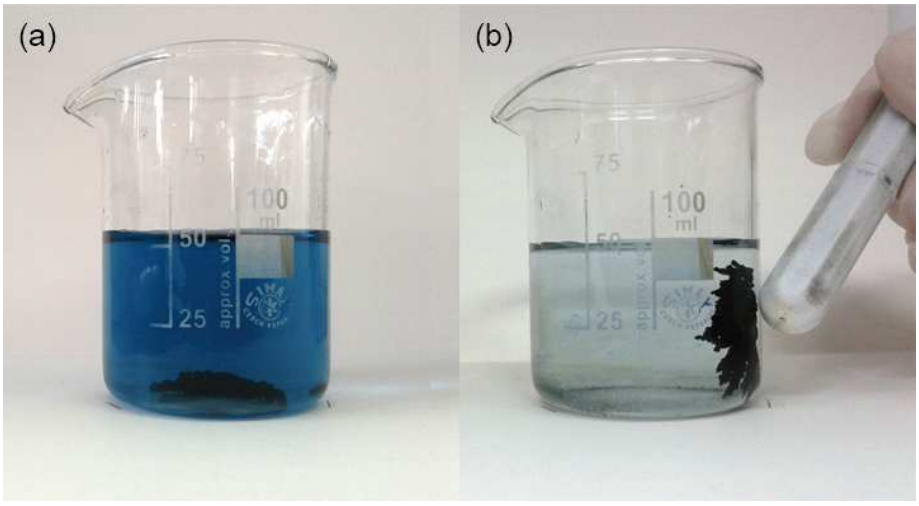

Fig. 9 Cs/PPy/Fe_3O_4 nanocomposite in the AG dye solution (a) before and (b) after adsorption. Fig. (b) demonstrates easy separation of Cs/PPy/Fe_3O_4 nanocomposite by magnet.

Table 1. Kinetics parameters for the adsorption of AG onto Cs/PPy/Fe_3O_4 nanocomposite.

Models	Model coefficient	R^2	χ^2
Pseudo-first order	Q_e = 26.238 mg g^{-1} k_1 = 0.074 min^{-1}	0.99677	0.002
Pseudo-second order	Q_e = 32.754 mg g^{-1} k_2 = 0.002613 g mg^{-1} min^{-1}	0.99552	0.009
Intraparticle diffusion	k_3 = 4.0599 mg g^{-1} $min^{1/2}$ C = 1.32808 mg g^{-1}	0.97542	1.483

Table 2. Isotherm parameters for the adsorption of AG onto Cs/PPy/Fe_3O_4 nanocomposite.

Models	Model coefficient	R^2
Langmuir model	a_ℓ = 0.8568561 L mg^{-1} K_ℓ = 47.619 L mg^{-1} 1/n = 0.42803	0.9492
Freundlich model	n = 2.336 K_f = 24.725 L mg^{-1}	0.95349
Temkin model	B = 12.186 J mol^{-1} K_t = 8.596 L mg^{-1}	0.9407

A table of contents

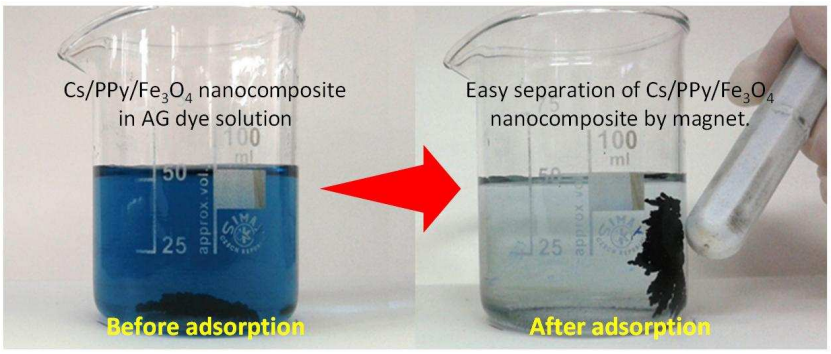

Chitosan/polypyrrole/magnetite nanocomposite is prepared via *in-situ* chemical polymerization of pyrrole using anhydrous $FeCl_3$ in the presence of chitosan.